Research Article | Vol. 29, No. 11 / 24 May 2021 / Optics Express 16857
Optics EXPRESS

Simulations of micro-sphere/shell 2D silica photonic crystals for radiative cooling

G. L. WHITWORTH,[1,4] J. JARAMILLO-FERNANDEZ,[1,5] J. A. PARIENTE,[2] P. D. GARCIA,[1] A. BLANCO,[2] C. LOPEZ,[2] AND C. M. SOTOMAYOR-TORRES[1,3]

[1]*Catalan Institute of Nanoscience and Nanotechnology (ICN2), CSIC and BIST, Campus UAB, Bellaterra, 08193 Barcelona, Spain*
[2]*Instituto de Ciencia de Materiales de Madrid (ICMM), c/Sor Juana Inés de la Cruz 3, 28049 Madrid, Spain*
[3]*Institucio Catalana de Recerca i Estudis Avancats (ICREA), 08010 Barcelona, Spain*
[4]*guy.whitworth@icfo.eu*
[5]*juliana.jaramillo@icn2.cat*

Abstract: Passive daytime radiative cooling has recently become an attractive approach to address the global energy demand associated with modern refrigeration technologies. One technique to increase the radiative cooling performance is to engineer the surface of a polar dielectric material to enhance its emittance at wavelengths in the atmospheric infrared transparency window (8–13 μm) by outcoupling surface-phonon polaritons (SPhPs) into free-space. Here we present a theoretical investigation of new surface morphologies based upon self-assembled silica photonic crystals (PCs) using an in-house built rigorous coupled-wave analysis (RCWA) code. Simulations predict that silica micro-sphere PCs can reach up to 73 K below ambient temperature, when solar absorption and conductive/convective losses can be neglected. Micro-shell structures are studied to explore the direct outcoupling of the SPhP, resulting in near-unity emittance between 8 and 10 μm. Additionally, the effect of material composition is explored by simulating soda-lime glass micro-shells, which, in turn, exhibit a temperature reduction of 61 K below ambient temperature. The RCWA code was compared to FTIR measurements of silica micro-spheres, self-assembled on microscope slides.

The global demand for cooling technologies represents an escalating problem in society, accounting for about 15% of global energy consumption and 10% of greenhouse gas emissions. As the world feels the effects of climate change, new and better cooling solutions will be required since these figures are predicted to triple by 2050 [1,2]. Cooling below ambient temperature is needed for a variety of refrigeration applications such as space cooling for human comfort and data centres [3–5]. On the other hand, above–ambient temperature cooling, i.e., the cooling of an object hotter than its surroundings, would enhance the efficiency of green power generation such as solar photovoltaics or thermoelectric modules, [6–8] which are temperature dependent and would benefit from passive cooling to maximise energy production [9,10].

The Earth maintains thermal equilibrium through the balance between absorbed solar energy and dissipated energy via thermal radiation, using the vast and cold outer space (3 K) as a heatsink. Current cooling technologies use the surrounding ambient environment (300 K) as a heatsink and, therefore, outer-space appears as a far more attractive, inexhaustible thermodynamic resource [11–13]. Heat can be directly exchanged from objects at the Earth's surface to outer space by means of thermal radiation. This provides a radiative heat transfer channel that can be exploited to achieve terrestrial passive radiative cooling. In this process, the atmosphere is the main limiting barrier, since it contains water vapour, carbon dioxide, ozone and other greenhouse gasses which partially absorb the outgoing long-wavelength radiation from the Earth's surface. This absorption of atmospheric molecules [14] results in further heating an object at the Earth's surface due

#420989 https://doi.org/10.1364/OE.420989
Journal © 2021 Received 10 Feb 2021; revised 1 Apr 2021; accepted 7 Apr 2021; published 17 May 2021

Optics EXPRESS

to the infrared radiation emitted by the atmosphere (by Kirchhoff's law of thermal radiation). However, between 8 and 13 μm, the atmosphere has a distinctive infrared transparency window where radiation from the surface can reach to the cold outer space without being absorbed. The net radiative heat flux to outer space from an object at the Earth's surface is thus limited by the incident thermal radiation from the atmosphere and the absorbed sunlight. Therefore, in order to achieve efficient radiative cooling on Earth, surfaces with high emittance in the atmospheric transparency window that neither absorb the incoming solar radiation nor thermal radiation from the ambient atmosphere must be engineered. Many such radiative cooling materials have now been demonstrated using nanopatterning technologies and surface engineering to maximize this process, promising a viable cooling technology for massive global energy savings [15–19].

For radiative cooling, two main types of material designs are studied: selective emitters, which have extremely high emittance in the atmospheric IR transparency window (8–13 μm) but close to zero over all other wavelengths, and broadband emitters which radiate over the entire infrared spectral region (>2.5 μm) [13,14]. While selective emitters are the preferred choice for cooling surfaces below the ambient temperature due to their lower absorbed incoming radiation, broadband emitters drop the requirement for limiting atmospheric absorption in favour of high spectral emittance in a broad wavelength range. Therefore, broadband emitters are primarily useful in above-ambient conditions where they can overcome the absorbed atmospheric radiation with higher radiated power due to their blackbody emission. Figure 1(a) shows the ideal emittance of perfect broadband (black) and selective (red) emitters, as well as the atmospheric transmittance (purple) for clear, dry conditions (water column = 1 mm, obtained from the Gemini Observatory IR transmission data [20]) and the normalised solar irradiance at AM1.5 (yellow). In addition, the normalised blackbody spectrum at 300 K is plotted (green). It can be seen that the blackbody radiation peak overlaps with the centre of the IR atmospheric transparency window. With these emittance/transmittance spectra, the net cooling power (P_{cool}) of a surface can be calculated as a function of its temperature (T_r) and the ambient temperature (T_{amb}), using the following equation:

$$P_{cool}(T_r,\ T_{amb}) = P_{rad}(T_r) - P_{atm}(T_{amb}) - P_{sun} - P_{cond+conv}(T_r,\ T_{amb}) \tag{1}$$

Where P_{rad} is the radiated power due to the surface blackbody emission, P_{atm} is the absorbed blackbody radiation of the ambient atmosphere, P_{sun} is the absorbed solar power and $P_{cond+conv}$ is the environmental heating due to conduction and convection. The latter term is a linear function proportional to the temperature difference between the emitting surface and the ambient temperature, for which the constant of proportionality is denoted as h_c (detailed expressions for each term can be found in Supplement 1) [12,21].

The net cooling power of thermal emitters under "perfect" conditions with no solar absorption ($P_{sun} = 0$) and/or non-radiative losses ($P_{cond+conv} = 0$) is calculated with Eq. (1). This is shown in Fig. 1(b), along with a typical solar absorption of 3% ($P_{cond+conv} = 0$) and conduction and convection losses ($h_c = 6.9\ W/m^2K$ and $P_{sun} = 0$), plotted as a function of the difference between ambient and radiative cooler temperatures. The value of $h_c = 6.9\ W/m^2K$ and the 3% solar absorption were taken from previous reports on radiative sky cooling to represent realistic conditions [21,22]. It is noteworthy that this is a simplified model which does not consider the temperature variation across the different layers of the atmosphere. Ideal broadband emitters outperform their selective counterparts at high temperatures (Supplement 1, Fig. S1), however, for below-ambient cooling the selective emitters perform better than the broadband ones, reaching 86 K below the ambient temperature before having a net cooling power of zero, in comparison to 44 K for the broadband emitters under "perfect" conditions (Fig. 1(b)). When the net cooling power is equal to zero, the temperature of the emitter stabilizes at a temperature, $T_r|_{P_{cool}=0}$. The temperature difference between the emitter at this point, and the ambient temperature is from here on used to characterise the below-ambient cooling performance of the surfaces and is defined as $\Delta T = T_{amb} - T_r|_{P_{cool}=0}$. Heating from solar absorption hinders

Optics EXPRESS

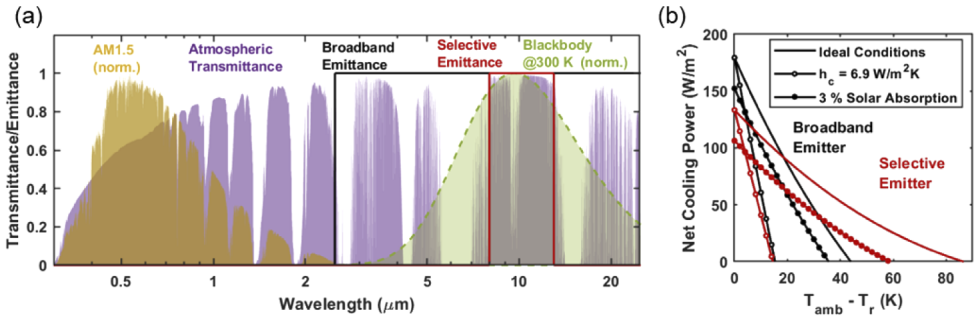

Fig. 1. Atmospheric conditions and radiative coolers. (a) Spectra depicting the normalised AM1.5 solar irradiance (orange), the atmospheric transmittance for dry conditions (water column = 1mm) (purple), the ideal broadband emittance spectrum (black), the ideal selective emittance spectrum (red) and the normalised blackbody irradiance at 300 K (green). (b) Predicted net cooling power, P_{cool}, of ideal broadband and selective radiative coolers obtained using Eq. (1) and the displayed atmospheric transmittance in (a), for three different conditions: zero convection and zero solar absorption (solid-lines); 3% solar absorption only (filled circles); and convection/conduction losses only (open circles), with a convection and conduction coefficient h_c of 6.9 W/m^{2}K. T_{amb} and T_r refer to the ambient and radiative cooler temperatures, respectively.

the radiative cooling performance of the device. Additionally, in the case of below-ambient cooling, conduction/convection drive the temperature of the emitter towards that of the ambient. Thus, to achieve a maximum below-ambient radiative cooling, it is necessary to design a structure with negligible absorption in the visible, reflecting the solar irradiance from 0.3 to 2.5 μm and to have an architecture which minimises convective and conductive losses ($h_c \cong 0$) as demonstrated by Chen et al. [23].

In order to design and optimise a structure for radiative cooling, an appropriate material must be chosen with high emittance in the IR transparency window. Fused silica (f-SiO_2) is a seemingly poor choice for a radiative cooler as it is highly reflective in the desired region due to its bulk phonon-polariton band. This band, also known as the Reststrahlen band [24], is a spectral region between the longitudinal and transverse optical phonon frequencies, where the real part of the permittivity takes negative values. Electromagnetic radiation with frequencies within that range cannot propagate through the material, causing a metallic-like reflectance band gap [25] (See Supplement 1, Figs. S2 and S3). However, when bulk silica is reduced to small particles, e.g. in the form of sand, this reflectivity band disappears and is replaced with high emissivity for particle sizes in the micrometer range [26,27]. This occurs partly due to the outcoupling of surface phonon-polariton (SPhP) states, which are quantum mechanical waves that can couple to and from free-space in a similar way to that of surface-plasmons. When a polar dielectric material is formed into small particles or is structured at the micro/nanoscale, the outcoupling of SPhP states can be maximised compared to the bulk [16,25,28–32]. Another feature that contributes to the suppression of the reflectance band is the spherical geometry of the particles, which reduces the impedance mismatch between air and f-SiO_2, and induces localized surface resonant modes. These features can be combined resulting in high emittance within the atmospheric IR transparency window, therefore exhibiting a selective spectral profile, which in turn can be exploited to fabricate selective emitters for radiative cooling.

In this work, we theoretically investigate the radiative cooling performance of new surface morphologies in the form of silica micro-sphere and micro-shell photonic crystals (PCs). To calculate their emittances, we use Kirchhoff's law of thermal radiation whereby the spectrally and angular dependent emittance is equal to the spectrally and angular dependent absorptance,

Optics EXPRESS

$\epsilon(\lambda, \theta, \phi) \equiv \alpha(\lambda, \theta, \phi)$, under thermal equilibrium [33]. The absorptance (and therefore emittance) can be calculated using electromagnetic (EM) solvers by first computing the reflectance and transmittance, and then taking the difference from unity. The EM solver chosen for this work was an in-house built rigorous coupled-wave analysis (RCWA) code, written in MATLAB. RCWA is a Fourier-space electromagnetic solver describing how periodic structures scatter light into the spatial harmonics of sequential layers, used to obtain reflectance and transmittance.

Three structures were chosen to investigate how to maximise the SPhP emission, which can be fabricated using colloidal self-assembly methods. The structures simulated were simple hexagonal photonic crystals of fused SiO_2 spheres (Fig. 2(a)), fused SiO_2 shells and soda-lime shells (Fig. 2(b)). Micro/nano-sphere PCs are fabricated by a self-assembly process from a colloidal suspension and shell-based PCs by coating the PC, made by polymer spheres, with silica and subsequently dissolving away the polymer spheres [34,35]. In order to make selective emitters, the structures were simulated on silver which would act as a nearly perfect reflector in the visible to eliminate the solar power absorbed ($P_{sun} = 0$). The structures were modelled as infinitely periodic in the x- and y-directions and discretised into layers in the z-direction, performing a staircase approximation of the 3D structure (as illustrated in Figs. 2(a)–2(b)). The simulations were parameterised as a function of wavelength, λ, and polar angle, θ. The emittance was not observed to vary with the azimuthal angle, ϕ, and so was assumed to be constant in this dimension. The results obtained with the RCWA code were benchmarked against bulk reflectance measurements of SiO_2 and soda-lime glass from the literature [36] and experimental FTIR spectra of colloidal SiO_2 microsphere arrays deposited on a microscope slide (Supplement 1, Fig. S2).

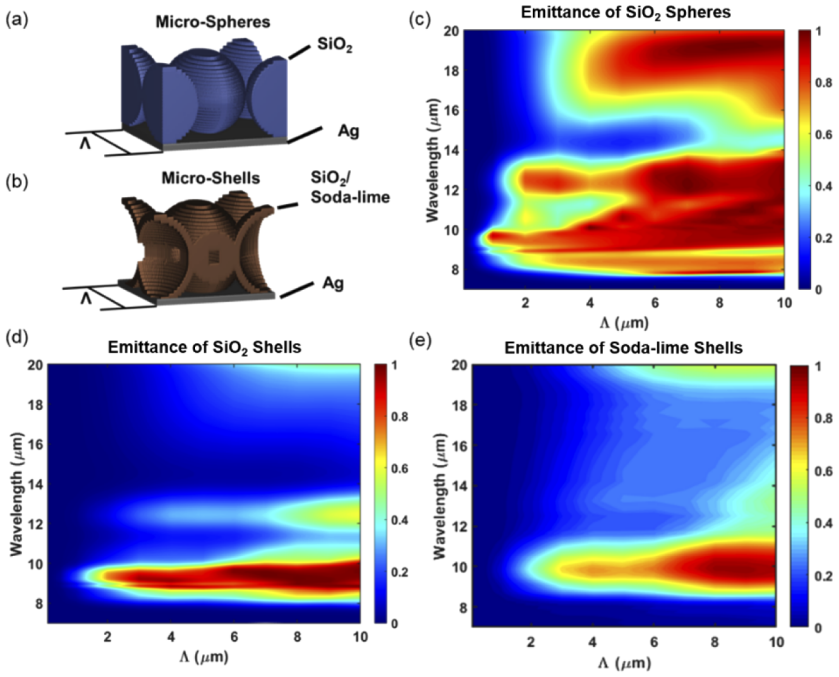

Fig. 2. Calculated size-dependent spectral emittances. (a) and (b) show the discretisation of the spheres and shells, respectively, used in the RCWA calculations. Both types of photonic crystals are simulated on top of silver. The predicted emittance spectra in the IR transparency window are plotted for (c) silica spheres, (d) silica shells and (e) soda-lime shells, as a function of wavelength and periodicity, Λ.

Optics EXPRESS

The colour plots in Figs. 2(c)–2(e), show the results for the calculated emittance normal to the surface, as a function of wavelength and the photonic crystal period, Λ, for the three simulated cases. The data of 1 mm thick slabs of fused silica and soda-lime glass can be found in Supplement 1 for comparison (Fig. S2), where the Reststrahlen band can be observed between 8 and 10 µm as a peak in reflectance (or a dip in absorptance/emittance). For the f-SiO_2 micro-sphere PC (Fig. 2(c)), a high emittance from 8 to 10 µm arises as the sphere diameter Λ, is increased. This is in stark contrast to the high reflectance characteristic of bulk f-SiO_2 within the Reststrahlen band region. There is also a strong emittance peak at 12.5 µm attributed to the permittivity of the bulk parent material. At $\Lambda \geq 6$ µm, the combination of these peaks results in high emittance across the atmospheric transparency window. Accompanying this selective emittance, there is also a second emittance band at higher wavelengths beyond 16 µm due to a second Reststrahlen band centred at 21 µm (Supplement 1, Figs. S2 and S3) which is a deviation of the emittance spectra from the "ideal" selective emitter. However, there is a secondary IR atmospheric transparency window in this region which can additionally contribute to the net cooling power. For example, for $\Lambda \geq 5$ µm silica micro-spheres at ambient temperature, 17% of the net cooling comes from wavelengths between 16 and 20 µm.

In order to decouple the emittance due to surface phonon polaritons from that of intrinsic SiO_2 emittance, the SiO_2 shells were simulated (Fig. 2(b)) to remove the contribution of the SiO_2 core. The shell thickness was set to be equal to 2% of the inner diameter of the shell. This thickness was chosen as a balance between reducing the contribution of material emittance and a realistic shell thickness achievable in their fabrication. Figure 2(d) shows the emittance of the silica micro-shell PC normal to the surface. A sharp, near unity emittance is seen between 8 and 10 µm and the emittance at longer wavelengths is dramatically reduced compared to the case of the micro-spheres. This narrow emittance between 8 and 10 µm is therefore attributed to the outcoupling of SPhPs on the surface of the SiO_2 micro-shells.

However, compared to a perfect selective emitter that maximizes below-ambient cooling, the silica micro-shells still exhibit suboptimal values of emittance in the 10–13 µm range. In an attempt to improve emittance in this range to encompass the full IR atmospheric transparency window, another set of PC shells were simulated, this time made from soda-lime glass instead of fused SiO_2. Soda-lime glass is the most prevalent form of glass consisting of SiO_2 but with oxide impurities, mainly Na_2O and CaO. Simulations of bulk soda-lime glass (Supplement 1, Figs. S2 and S3) show that these impurities reduce the Reststrahlen band compared to that of pure f-SiO_2, resulting in a relatively acceptable broadband radiative cooler. As predicted, the soda-lime shells exhibited a broader emittance peak in the IR atmospheric transparency window (Fig. 2(e)) compared to that of the SiO_2 shell PC counterpart, attributed to surface electromagnetic modes and to the different chemical compositions. However, even with these thin shells of soda-lime glass, a relatively large contribution of the emittance that arises from the permittivity of the bulk parent material was found to be present at wavelengths longer than 13 µm.

To analyse the performance of these structures as selective radiative coolers, the emittance spectra were used to calculate the net cooling power as a function of temperature difference to the ambient ($T_{amb} = 300\ K$) using Eq. (1). The selective cooler figure of merit, was chosen to be the temperature difference ΔT between the ambient temperature and the emitting surface, at which the net cooling power is equal to zero as defined above. In Figs. 3(a)–3(b), ΔT is plotted as a function of photonic crystal period, i.e, the outer diameter of micro-spheres and the inner diameter of micro-shells, for two cases, $h_c = 0$ and $h_c = 6.9\ W/m^2K$. In both cases the solar absorption term is assumed to be zero, due to the high reflectance in the visible of the thin layer of structured silica on silver. Additionally, ΔT for f-SiO_2 and soda-lime bulk materials (1 mm), backed with silver is plotted for comparison.

In Fig. 3 it is seen that all three 2D arrays outperform their bulk counterparts as selective coolers under "perfect" conditions, namely, zero solar absorption and zero conduction and

Optics EXPRESS

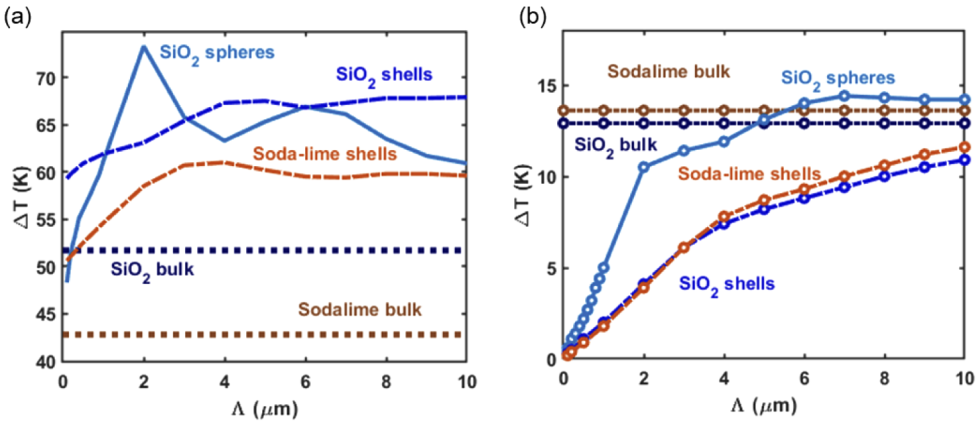

Fig. 3. Radiative cooling performance of simulated structures. Temperature difference between the ambient temperature and the emitting surface, at which the radiative cooling power is equal to zero ($\Delta T = T_{amb} - T_r|_{P_{cool}=0}$) for the three micro structures and the two bulk materials, as a function of the micro-sphere/shell diameter, (a) under "perfect" conditions (zero convection/conduction and zero solar absorption) and (b) with a convection and conduction coefficient of 6.9 W/m^{2}K.

convection losses, with the f-SiO_2 micro-spheres performing best. The micro-sphere array reaches a maximum temperature difference of $\Delta T \simeq 73$ K below ambient for 2 µm diameter spheres. For micro-sphere PCs with higher diameters, the net cooling power decreases as more emittance outside the transparency window increases. This decrease is not observed in the micro-shells, which showed a continual increase in net cooling power with increasing diameter up to $\Delta T \simeq 68$ K at $\Lambda = 10$ µm. The soda-lime micro-shells exhibited a similar behaviour as that of the silica micro-shells although with lower performance attributed to their higher emittance outside the atmospheric transparency window, reaching a maximum temperature difference of 61 K below ambient ($\Lambda = 4$ µm). Figure 3(b) shows the results for the same structures this time including convection and conduction heat transfer ($h_c = 6.9\ W/m^2K$). In these less-than-ideal circumstances only the silica micro-spheres outperform the bulk material, resulting in a temperature difference of 15 K below ambient at $\Lambda = 7$ µm. This is because larger spheres exhibit a higher broadband emittance. As shown in Fig. 1(b), perfect broadband emitters show a smaller net cooling power reduction than perfect selective coolers when conduction and convection losses are introduced. The micro-shells show a much smaller ΔT when convection and conduction heating is considered, due to their narrower emission.

The best radiative cooling cases for zero convective and conductive heating and zero solar absorption were 2 µm silica micro-spheres, 10 µm silica micro-shells, and 4 µm soda-lime micro-shells. Figure 4(a) shows the emittance spectra normal to the surface of the three cases and the atmospheric transmittance. The 2 µm silica spheres achieve high emittance coverage of the atmospheric window, averaging at 0.65 for a broad range of angles (Fig. 4(b)). Despite having comparable emittance coverage (0.60–0.70), the silica 10 µm shells achieve lower net cooling power compared to that of the spheres. This is believed to be due to the high emittance at the ozone (O_3) atmospheric absorption line at 9.5 µm, leading to a higher value for the absorbed ambient radiation (P_{atm}). The low emittance across the atmospheric window (0.50) and the relatively high atmospheric absorptance, limit the radiative cooling performance of the soda-lime shells when compared to the silica shell.

Further analysis of the angle-dependent emittance of these three cases sheds light onto the underlying physics behind the enhanced emittance (Fig. 5). The p-polarised emittance has been

Optics EXPRESS

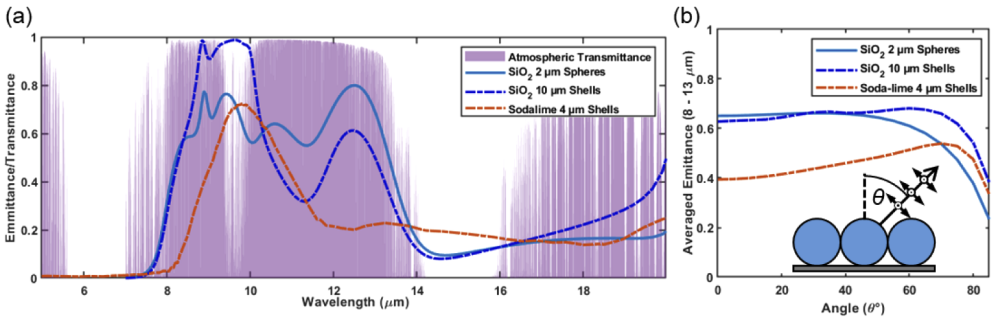

Fig. 4. Unpolarised angle-dependent spectral emittance (a) Emittance spectra of the silica spheres, silica shells, and the soda-lime shells for sizes which showed the highest value of ΔT for each case: 2 μm, 10 μm and 4 μm, respectively. The atmospheric transmittance profile is superimposed. (b) The average emittance of the three mentioned cases in the atmospheric transparency window (8–13 μm) as a function of angle.

plotted in Fig. 5 and s-polarisation data can be found in Supplement 1, Fig. S4. Black dotted lines indicate the wavelengths at which the real part of the dielectric constant is equal to zero, 8 μm and 9.3 μm for silica and, 8.9 μm and 9.7 μm for soda-lime. The wavelengths correspond to the longitudinal (LO) and transverse (TO) optical phonon frequencies, respectively i.e., these are the frequencies at which longitudinal and transverse oscillations of the ions in the material are resonant. All three cases show a strong emittance just above the TO mode for a large range of angles, accounting for the majority of emittance improvement in the simulations. Furthermore, for the silica micro-spheres, a high emittance peak is observed at the resonant frequency of the longitudinal optical phonon mode at 35° (Fig. 5(b)). For the silica structures, spheres and shells, a sharp, non-dispersive resonance is present between the optical phonon frequencies at 8.9 μm. This is attributed to the direct outcoupling of the surface-phonon polaritons. The same SPhP resonance is not present in the soda-lime micro-shells due to the "weaker" Reststrahlen band.

In conclusion we predict that spherical silica micro-structures on a surface reflecting the solar irradiance from 0.3 to 2.5 μm (in this case silver) have a great potential for below-ambient radiative cooling applications, especially under set-up designs that limit conduction and convection losses. Structures were characterised by the maximum temperature difference between the cooler and the ambient that can be achieved by passive radiative cooling i.e., when the net cooling power becomes equal to zero ($\Delta T = T_{amb} - T_r|_{P_{cool}=0}$). When solar absorption and conductive/convective losses were not considered, silica micro-spheres and silica micro-shells PCs reached temperatures of 73 K and 67.9 K below ambient, respectively. Silica micro-shells are seen to exhibit extremely narrow thermal emission between 8 and 10 μm attributed primarily to the surface phonon-polariton outcoupling from the structures to free-space. This could form a narrowband thermal IR source for photonic applications [17,37]. Soda-lime glass micro-shell PCs were investigated in an attempt to improve the narrow-band emittance achieved using f-SiO_2, such that it could encompass the full IR atmospheric transparency window. Despite the broadened emittance in the targeted spectral range resulting from the impurities present in this type of glass, lower net cooling power and a higher below ambient temperature of 61 K were achieved, due to the higher atmospheric absorption. Finally, the angle-dependent emittance of the proposed structures has been analysed, and the results suggest that the strong emittance of the three PCs is mainly due to surface electromagnetic modes and partly due to SPhP outcoupling in the case of pure f-SiO_2 structures. Our work presents the potential of a material platform for below-ambient radiative cooling applications that is simple, cost-efficient, can be mass-produced and avoids the use of plastics.

Optics EXPRESS

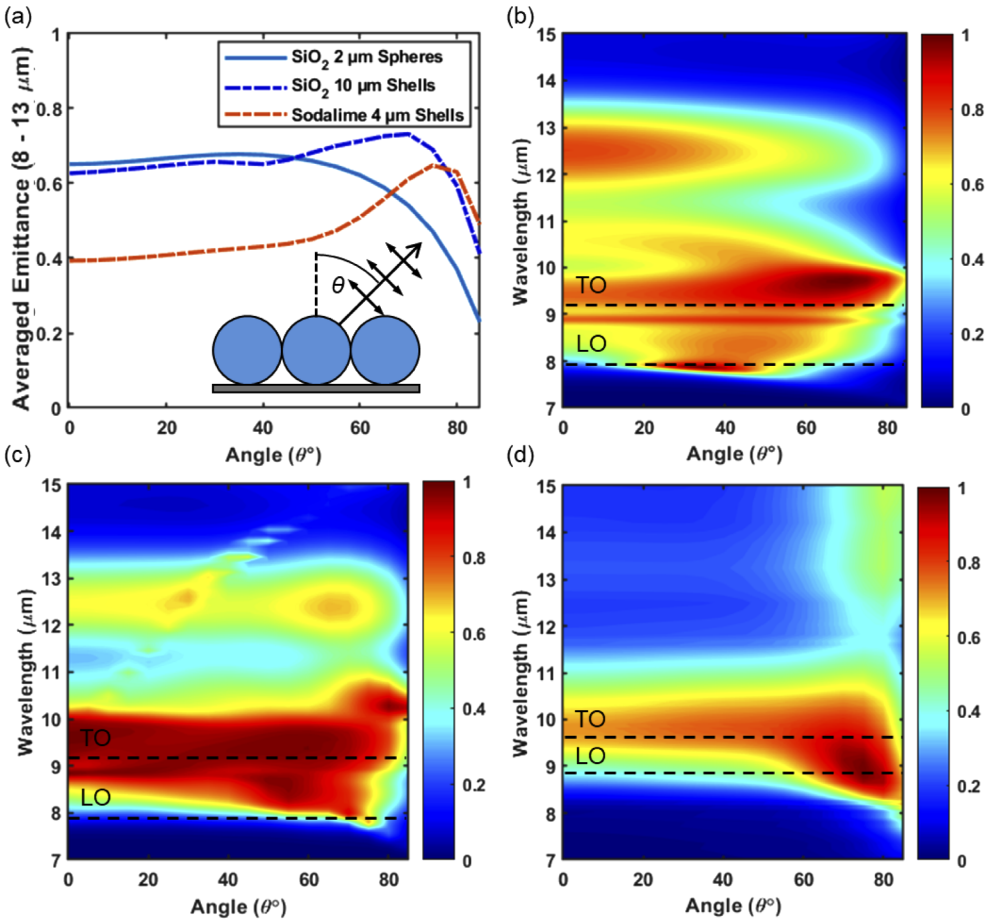

Fig. 5. p-polarised directional spectral emittance (a) The p-polarised average emissivity of the three considered best cases across the atmospheric transparency window (8–13 μm). Directional spectral emittance in the p-polarisation of (b) 2 μm silica spheres, (c), 10 μm silica shells, and (d), 4 μm soda-lime shells. Dotted lines indicate at which wavelength the dielectric constant is zero for the respective material.

Funding. Horizon 2020 Framework Programme (721062); H2020 Marie Skłodowska-Curie Actions (665919); Ministerio de Ciencia, Innovación y Universidades (PGC2018-101743-B-I00, RTI2018-093921-B-C41, SEV-2017-0706, RTI2018-093921-B-44, RyC-2015-18124, FPI programme); Centres de Recerca de Catalunya.

Acknowledgments. The European Union's Horizon 2020 Research and Innovation Program funded this research under the project FLEXPOL (GA. Nr 721062) that supported G.L.W. and the Marie Sklodoswa-Curie Actions Grant No. 665919 that supported J.J.-F. Moreover, the research received funds from the Spanish Minister of Science, Innovation and Universities via the Severo Ochoa Program (Grant No. SEV-2017-0706) that supports ICN2, and the projects PGC2018-101743-B-I00 (SIP), RTI2018-093921-B-C41 and RTI2018-093921-A-C44 (SMOOTH), as well as by the CERCA Program/Generalitat de Catalunya. P.D.G. was supported by a Ramon y Cajal Fellowship No. RyC-2015-18124 and J.A.P. acknowledges MICIU FPI programme.

Disclosures. The authors declare no conflicts of interest.

Data availability. Data underlying the results presented in this paper are not publicly available at this time but may be obtained from the authors upon reasonable request.

Supplemental document. See Supplement 1 for supporting content.

References

Optics EXPRESS

1. U. S. D. of Energy, *Residential Energy Consumption Survey (RECS)* (2015).
2. Intergovernmental Panel on Climate Change, *Climate Change 2014 Mitigation of Climate Change* (2014).
3. S. Vall and A. Castell, "Radiative cooling as low-grade energy source: A literature review," Renew. Sustain. Energy Rev. **77**, 803–820 (2017).
4. R. Family and M. P. Mengüç, "Materials for Radiative Cooling: A Review," Procedia Environ. Sci. **38**, 752–759 (2017).
5. G. Smith and A. Gentle, "Radiative cooling: Energy savings from the sky," Nat. Energy **2**(9), 17142 (2017).
6. W. Li, Y. Shi, K. Chen, L. Zhu, and S. Fan, "A Comprehensive Photonic Approach for Solar Cell Cooling," ACS Photonics **4**(4), 774–782 (2017).
7. D. Sato and N. Yamada, "Review of photovoltaic module cooling methods and performance evaluation of the radiative cooling method," Renew. Sustain. Energy Rev. **104**, 151–166 (2019).
8. B. Zhao, M. Hu, X. Ao, and G. Pei, "Performance analysis of enhanced radiative cooling of solar cells based on a commercial silicon photovoltaic module," Sol. Energy **176**, 248–255 (2018).
9. L. Zhu, A. P. Raman, and S. Fan, "Radiative cooling of solar absorbers using a visibly transparent photonic crystal thermal blackbody," Proc. Natl. Acad. Sci. **112**(40), 12282–12287 (2015).
10. J. Jaramillo-fernandez, G. L. Whitworth, J. A. Pariente, A. Blanco, P. D. Garcia, C. Lopez, and C. M. Sotomayor-torres, "A Self-Assembled 2D Thermofunctional Material for Radiative Cooling," Small **15**(52), 1905290 (2019).
11. E. A. Goldstein, A. P. Raman, and S. Fan, "Sub-ambient non-evaporative fluid cooling with the sky," Nat. Energy **2**(9), 17143 (2017).
12. M. M. Hossain and M. Gu, "Radiative cooling: Principles, progress, and potentials," Adv. Sci. **3**(7), 1500360 (2016).
13. X. Sun, Y. Sun, Z. Zhou, M. A. Alam, and P. Bermel, "Radiative sky cooling: fundamental physics, materials, structures, and applications," Nanophotonics **6**(5), 997–1015 (2017).
14. C. G. Granqvist, "Radiative heating and cooling with spectrally selective surfaces," Appl. Opt. **20**(15), 2606–2615 (1981).
15. Y. Zhai, Y. Ma, S. N. David, D. Zhao, R. Lou, G. Tan, R. Yang, and X. Yin, "Scalable-manufactured randomized glass-polymer hybrid metamaterial for daytime radiative cooling," Science **355**(6329), 1062–1066 (2017).
16. X. G. Xu, B. G. Ghamsari, J. H. Jiang, L. Gilburd, G. O. Andreev, C. Zhi, Y. Bando, D. Golberg, P. Berini, and G. C. Walker, "One-dimensional surface phonon polaritons in boron nitride nanotubes," Nat. Commun. **5**(1), 4782 (2014).
17. E. Tervo, Z. Zhang, and B. Cola, "Collective near-field thermal emission from polaritonic nanoparticle arrays," Phys. Rev. Mater. **1**(1), 015201 (2017).
18. J. long Kou, Z. Jurado, Z. Chen, S. Fan, and A. J. Minnich, "Daytime Radiative Cooling Using Near-Black Infrared Emitters," ACS Photonics **4**(3), 626–630 (2017).
19. A. R. Gentle and G. B. Smith, "Radiative heat pumping from the Earth using surface phonon resonant nanoparticles," Nano Lett. **10**(2), 373–379 (2010).
20. G. Observatory, "IR Transmission Spectra," https://www.gemini.edu/sciops/telescopes-and-sites/observing-condition-constraints/ir-transmission-spectra.
21. M. Zeyghami, D. Y. Goswami, and E. Stefanakos, "A review of clear sky radiative cooling developments and applications in renewable power systems and passive building cooling," Sol. Energy Mater. Sol. Cells **178**, 115–128 (2018).
22. A. P. Raman, M. A. Anoma, L. Zhu, E. Rephaeli, and S. Fan, "Passive radiative cooling below ambient air temperature under direct sunlight," Nature **515**(7528), 540–544 (2014).
23. Z. Chen, L. Zhu, A. Raman, and S. Fan, "Radiative cooling to deep sub-freezing temperatures through a 24-h day-night cycle," Nat. Commun. **7**(1), 13729 (2016).
24. S. Adachi and S. Adachi, "The Reststrahlen Region," in *Optical Properties of Crystalline and Amorphous Semiconductors* (Springer, 1999).
25. J. D. Caldwell, L. Lindsay, V. Giannini, I. Vurgaftman, T. L. Reinecke, S. A. Maier, and O. J. Glembocki, "Low-loss, infrared and terahertz nanophotonics using surface phonon polaritons," Nanophotonics **4**(1), 44–68 (2015).
26. G. Masiello, C. Serio, S. Venafra, G. Liuzzi, F. Göttsche, I. F. Trigo, and P. Watts, "Kalman filter physical retrieval of surface emissivity and temperature from SEVIRI infrared channels: A validation and intercomparison study," Atmos. Meas. Tech. **8**(7), 2981–2997 (2015).
27. A. M. Baldridge, S. J. Hook, C. I. Grove, and G. Rivera, "The ASTER spectral library version 2.0," Remote Sens. Environ. **113**(4), 711–715 (2009).
28. S. Inampudi and H. Mosallaei, "Tunable wideband-directive thermal emission from SiC surface using bundled graphene sheets," Phys. Rev. B **96**(12), 125407 (2017).
29. C. G. Granqvist and A. Hjortsberg, "Radiative cooling to low temperatures: General considerations and application to selectively emitting SiO films," J. Appl. Phys. **52**(6), 4205–4220 (1981).
30. A. D. Dunkelberger, C. T. Ellis, D. C. Ratchford, A. J. Giles, M. Kim, C. S. Kim, B. T. Spann, I. Vurgaftman, J. G. Tischler, J. P. Long, O. J. Glembocki, J. C. Owrutsky, and J. D. Caldwell, "Active tuning of surface phonon polariton resonances via carrier photoinjection," Nat. Photonics **12**(1), 50–56 (2018).
31. P. Li, M. Lewin, A. V. Kretinin, J. D. Caldwell, K. S. Novoselov, T. Taniguchi, K. Watanabe, F. Gaussmann, and T. Taubner, "Hyperbolic phonon-polaritons in boron nitride for near-field optical imaging and focusing," Nat. Commun. **6**(1), 7507 (2015).

Optics EXPRESS

32. S. Dai, Z. Fei, Q. Ma, A. S. Rodin, M. Wagner, A. S. McLeod, M. K. Liu, W. Gannett, W. Regan, K. Watanabe, T. Taniguchi, M. Thiemens, G. Dominguez, A. H. Castro Neto, A. Zettl, F. Keilmann, P. Jarillo-Herrero, M. M. Fogler, and D. N. Basov, "Tunable phonon polaritons in atomically thin van der Waals crystals of boron nitride," Science **343**(6175), 1125–1129 (2014).
33. J. R. Howell, M. P. Mengüç, and R. Siegel, "Radiative Properties at Interfaces," in *Thermal Radiation Heat Transfer*, 6th ed. (CRC Press, 2015), pp. 51–85.
34. A. Blancao and C. López, "Silicon onion-layer nanostructures arranged in three dimensions," Adv. Mater. **18**(12), 1593–1597 (2006).
35. P. D. García, R. Sapienza, Á Blanco, and C. López, "Photonic glass: A novel random material for light," Adv. Mater. **19**(18), 2597–2602 (2007).
36. S. I. Amma, J. Luo, C. G. Pantano, and S. H. Kim, "Specular reflectance (SR) and attenuated total reflectance (ATR) infrared (IR) spectroscopy of transparent flat glass surfaces: A case study for soda lime float glass," J. Non. Cryst. Solids **428**, 189–196 (2015).
37. J. J. Greffet, R. Carminati, K. Joulain, J. P. Mulet, S. Mainguy, and Y. Chen, "Coherent emission of light by thermal sources," Nature **416**(6876), 61–64 (2002).